Published in final edited form as:
Small. 2010 September 20; 6(18): 2041–2049. doi:10.1002/smll.201000596.

A Light-activated Theranostic Nanoagent for Targeted Macrophage Ablation in Inflammatory Atherosclerosis

Dr. Jason R. McCarthy[†],
Center for Systems Biology, Harvard Medical School and Massachusetts General Hospital, 185 Cambridge Street, Suite 5.210, Boston, MA 02114, USA, Phone: 617-726-9218, Fax: 617-726-5708

Dr. Ethan Korngold[†],
Cardiovascular Research Center, Cardiology Division, Harvard Medical School and Massachusetts General Hospital, 185 Cambridge St Room 3206, Boston MA 02114, USA

Dr. Ralph Weissleder, and
Center for Systems Biology, Harvard Medical School and Massachusetts General Hospital, 185 Cambridge Street, Suite 5.210, Boston, MA 02114, USA, Phone: 617-726-9218, Fax: 617-726-5708

Dr. Farouc A. Jaffer[*]
Cardiovascular Research Center, Cardiology Division, Harvard Medical School and Massachusetts General Hospital, 185 Cambridge St Room 3206, Boston MA 02114, USA

Jason R. McCarthy: jason_mccarthy@hms.harvard.edu; Farouc A. Jaffer: fjaffer@mgh.harvard.edu

Abstract

The synthesis and utility of a multimodal theranostic nanoagent based upon magnetofluorescent nanoparticles for the treatment of inflammatory atherosclerosis is described. These particles are modified with near-infrared fluorophores and light-activated therapeutic moieties, which allow for the optical determination of agent localization and phototoxic activation at spectrally distinct wavelengths. The resulting agent is readily taken up by murine macrophages in vitro, and is highly phototoxic, with an LD_{50} of 430 pM. Intravenous administration results in the localization of the nanoagent within macrophage-rich atherosclerotic lesions that can be imaged by intravital fluorescence microscopy. Irradiation of the atheroma with 650 nm light in order to activate the therapeutic component results in eradication of inflammatory macrophages, which may induce lesion stabilization. Importantly, these agents display limited skin photosensitivity, are highly efficacious, and provide an integrated imaging and therapeutic nanoplatform for atherosclerosis.

Keywords

atherosclerosis; imaging; macrophage; multimodal; photodynamic therapy; theranostic

1. Introduction

The sequelae of atherosclerotic vascular disease are the leading causes of death and disability in the developed world.[1] It is thus imperative to develop novel techniques to

Correspondence to: Jason R. McCarthy, jason_mccarthy@hms.harvard.edu; Farouc A. Jaffer, fjaffer@mgh.harvard.edu.

[†]Drs. McCarthy and Korngold contributed equally to this work.

detect and treat atherosclerotic lesions prior to the onset of symptoms. Over the past decade, the role of the innate immune response in the initiation and progression of atherosclerosis has been elucidated.[2,3] In particular, the macrophage has emerged as a key component of atherogenesis, from foam cell and fatty streak formation to the generation of proteinases that lead to plaque destabilization and rupture.[2–5] Additionally, macrophages constitute up to 20% of the cells within atherosclerotic lesions, and as such, the macrophage may serve as an ideal target for the detection and therapy of vulnerable, inflamed lesions.[5]

A number of different nanomaterials have been synthesized that show high affinities for phagocytic macrophages, including dextran coated iron oxide nanoparticles.[6–9] In fact, these dextranated particles have previously been used clinically for the magnetic resonance (MR)-based detection of macrophage burden in atherosclerotic lesions.[9,10] One derivative that has been extensively studied relies upon the epichlorohydrin-induced crosslinking of the dextran coating around the iron oxide core.[11,12] When crosslinked dextran-coated iron oxide (CLIO) nanoparticles are injected into atherosclerotic plaque-laden apolipoprotein E deficient (apoE$^{-/-}$) mice, over 75% of the particles contained within the lesion were associated with macrophages, 20% were contained within neutrophils, and the remainder within lymphocytes, smooth muscle cells, and endothelial cells, albeit at much lower amounts per cell.[7] Thus, the intrinsic affinity of the CLIO nanoplatform for inflammatory macrophages can be utilized for the delivery of multimodal theranostic (diagnostic and therapeutic) nanoparticles to atherosclerotic lesions.

While most therapeutic approaches have involved the systemic administration of cytotoxic drugs, focal therapies, such as those which are light activated, allow for control of the localization of the therapeutic effect. Thus, nontargeted near infrared light activated photosensitizers have been investigated for the treatment of a number of diseases, including atherosclerosis and in-stent restenosis.[13] Herein, the synthesis of a theranostic nanoparticles based upon CLIO and targeted to inflamed, macrophage-rich atherosclerotic lesions will be described. This agent is modified with a near infrared fluorophore in order to enable fluorescence imaging, as well as a potent chlorin-based photosensitizer, each at spectrally distinct wavelengths. Furthermore, the macrophage ablative efficacy of the nanoagent will be investigated in vitro, and in vivo in a murine model of atherosclerosis.

2. Results and Discussion

2.1. Theranostic nanoagent synthesis

We have previously described a first generation near infrared light activated theranostic nanoagent, based upon CLIO.[14] This nanoscaffold was modified with AlexaFluor 750 for near infrared fluorescence imaging and a hydrophobic, yet conjugatable, *meso*-tetraphenylchlorin derivative. While the resulting agent was adequately phototoxic in vitro, the non-polarity of the photosensitizer decreased the total number of chlorins that could be conjugated to the particle surface before causing flocculation. In order to circumvent this and increase the overall phototoxicity of the nanoagent, we have developed a novel hydrophilic photosensitizers based upon *meso*-tetra(*m*-hydroxyphenyl)chlorin, which allow for the conjugation of at least 3-fold more dyes per particle, while retaining suspension stability.

The utilized *meso*-hydroxyphenylchlorin derivative was synthesized from *meso*-tetra(*m*-methoxyphenyl)porphyrin **1** as depicted in Scheme 1. To the porphyrin in trifluoroacetic acid (TFA) was added 1.8 equiv $NaNO_2$, which was allowed to react for 4 min. This allows for the addition of a single nitro group to the *para*-position of one of the *meso*-(*m*-methoxyphenyl) substituents. After workup, the crude nitrated porphyrin **2** was subjected to $SnCl_2{\cdot}2H_2O$ reduction to the corresponding amine **3**. This amine was utilized to facilitate

the addition of a carboxylic acid functionalized linker moiety. Microwave assisted reaction of **3** with mono-fluorenylmethyl-protected glutaric acid (**Fm-Glu**)[15] in the presence of dicyclohexylcarbodiimide (DCC) yielded porphyrin **4**, which was then subjected to OsO_4-mediated dihydroxylation to give chlorins **5I** and **5II**.[16] This conversion of porphyrin to chlorin is highly important, with regard to the overall singlet oxygen generation, as it results in a chromophore with 10-fold greater absorption of the farthest red side band, which subsequently allows for 10-fold greater generation of the cytotoxic species. Unfortunately, due to the symmetry of the molecule, this conversion results in 4 isomers (2 regioisomers consisting of 2 stereoisomers each, Figure 1). These regioisomers are readily separable, and have identical photophysical properties. Demethylation of the *m*-methoxyphenyl groups with BBr_3, followed by fluorenylmethyl deprotection with 20% pipiridine in dimethylformamide yields the conjugatable *meso*-tetra(hydroxyphenyl)chlorin derivatives, **6I** and **6II**, which can be further activated for reaction with amines via succinimidyl ester formation (**7I** and **7II**). The product possesses a furthest red absorption at 648 nm, with an extinction coefficient of 1.6×10^4 L mol^{-1} cm^{-1}, and a singlet oxygen quantum yield of 0.6. The photophysical properties of **6I** and **6II** are comparable to the previously synthesized first generation chlorin.[14]

The nanoagent was synthesized by the modification of aminated crosslinked dextran-coated iron oxide nanoparticles.[11] Initially, the particle was reacted with AF750 (abs 753, em 782 nm) in order to impart upon the agent the ability to fluorescently image localization at a wavelength spectrally distinct from the therapeutic wavelength (650 nm, Figure 2). Reaction with the succinimidyl ester of AF750, followed by filtration through Sephadex G-25 yielded 3 AF750 per nanoparticle (**CLIO-AF750**). At this point, the **CLIO-AF750** was split into two portions, half of which was subsequently reacted with **7I** and filtered through Sephadex G-25 to give the product, **CLIO-THPC**, with approximately 30 chlorins per nanoparticle. The other half of the **CLIO-AF750** was retained as a fluorescence matched non-phototoxic control particle for use in the in vivo studies. The nanoparticle loading was determined spectrophotometrically using the extinction coefficients of the respective dyes. As was hypothesized, the increased polarity of the photosensitizer allowed for the inclusion of three times more chlorins. Particle size and polydispersity were subsequently determined by dynamic light scattering in order to assess the quality of nanoparticles. As compared to the CLIO starting material (49.9 nm diameter, 0.22 polydispersity index), neither **CLIO-AF750** nor **CLIO-THPC** demonstrated significant changes in size or polydispersity. This can be attributed to the fact that, on average, only 33 small molecules were conjugated to the nanoparticle's polymeric coating. Importantly, the nanoagents are stable in suspension for up to one year without appreciable flocculation or change in their photophysical properties.

2.2. In vitro uptake and phototoxicity

Cellular uptake of the macrophage-targeted theranostic nanoagent was investigated in RAW 264.7 murine macrophages in vitro. Incubation of **CLIO-THPC** with the macrophages resulted in significant cell-associated fluorescence, as can be seen in Figure 3. Irradiation of the cells with a 650 nm laser (50 mW cm^{-2}, 3 min) resulted in exceptional cell death. As compared to the commonly used chlorin e_6, which demonstrated an LD_{50} of 800 nM in the RAW cells, **CLIO-THPC** was almost sixty times more phototoxic (LD_{50} of 14 nM) on a chlorin-per-chlorin basis, and 1900-fold more toxic on a molecular level (per nanoparticle, LD_{50} of 430 pM). Importantly, at all concentrations tested, **CLIO-THPC** did not demonstrate any in vitro toxicity in the absence of light, whereas **CLIO-AF750** does not display phototoxicity at any concentration.

2.3. In vivo localization and therapy

The in vivo localization of the nanoagent to atherosclerotic lesions was next examined in apolipoprotein E deficient (apoE$^{-/-}$) mice. These genetically modified mice spontaneously develop atheromata that is accelerated by hypercholesterolemia. ApoE $^{-/-}$ mice on 10 weeks of high cholesterol diet were intravenously injected with **CLIO-THPC** or the control agent, **CLIO-AF750**. The agents were allowed 24 h to localize to the plaques, at which time the carotid arteries were surgically exposed in order image the nanoagent by intravital fluorescence microscopy (IVFM)[8,17] For both **CLIO-THPC** and the control agent, the atherosclerotic lesions demonstrated significant fluorescence in the AF750 channel (Figure 4A). During the imaging session, the mice were also injected with fluorescein-labeled dextran in order to visualize the vasculature (Figure 4B). Interestingly, a filling defect is readily observed in the fluorescein channel, which correlated well with the location of the lesion and the fluorescence from the **CLIO-THPC**.

After the initial imaging session, one cohort of mice was sacrificed, and the carotid arteries were resected and sectioned for histological examination by conventional (hemotoxylin and eosin staining, H&E) and correlative fluorescence microscopy. As can be seen in Figure 5, focal nanoparticle NIR fluorescence (stemming from the attached AF750 fluorochrome) is evident in the superficial cellular regions of inflamed plaques. The deposition pattern confirmed that the NIR fluorescence was nanoparticle specific and not due to autofluorescence of the atheroma. The agent clearly accumulated within the plaques, particularly those areas rich in macrophages and foam cells (Figure 5D). This result is not unexpected, as previous experience with this nanoparticulate scaffold has shown preferential uptake by these phagocytic cells.[6–8] In addition, histological inspection of these cells revealed that many of the these cells possessed condensed nuclei, consistent with photoxicity-induced plaque cell apoptosis.

To elicit a therapeutic effect, the exposed carotid arteries of the other cohorts of mice were irradiated with 650 nm laser light (150 mW, 3 min) in order to excite the macrophage-targeted photosenstitizer. Following light treatment, the surgical incisions were closed and the mice were allowed to recuperate. Twenty-four hours later, the mice were sacrificed and the carotid arteries were examined histologically. Sections were stained with hematoxylin and eosin (H&E), with sister sections stained with a terminal deoxynucleotidyl transferase dUTP nick end labeling stain (TUNEL), which labels cells undergoing apoptosis. As seen in Figure 6, a significant number of apoptotic cells cell were observed in the **CLIO-THPC** treated mice (55.5 ± 5.1 % of the plaque area), as compared to mice treated with **CLIO-AF750** (0.796 ± 0.10 % of the plaque area). This finding is consistent with macrophage delivery of the phototoxic photosensitizer on the **CLIO-THPC** nanoagent. Importantly, the apoptotic cells in Figure 6 co-localize with Mac-3 positive cells from sister sections, demonstrating the macrophage avidity of the agent in vivo.

2.4. Skin Phototoxicity

A detrimental aspect of photodynamic therapies can be unintended skin phototoxicity associated with the administration of relatively hydrophobic photosensitizers. As the utilized nanoscaffold does not demonstrate localization to the skin, we hypothesized that the agent would demonstrate negligible skin phototoxicity. In order to investigate this effect, we utilized a hind-paw edema model previously developed by Peng *et al*.[18] Initially, the left and right paws of each animal were measured with a digital caliper in order to measure the paw thickness. The mice were then injected with **CLIO-THPC** or the conventional photosensitizer, chlorin e_6, which were allowed either 1 h or 24 h to circulate, depending upon the cohort, at which point the right paw of the animals was irradiated with the 650 nm laser (150 mW, 3 min). Twenty four hours after irradiation, the footpad measurements were

repeated, and swelling was determined as a change in thickness (Figure 7). In the group that was irradiated 1 h after injection, **CLIO-THPC** displayed a minimal amount of edema (8 ± 5% change) while the chlorin e_6 group demonstrated a 4-fold greater change in thickness (32 ± 9%). Interestingly, in the groups that were irradiated 24 h after injection, the chlorin e_6 group showed a 14 ± 3% increase in paw thickness, while the **CLIO-THPC** group showed negligible change (−7 ± 9%) in paw thickness. This result further demonstrates the advantageous delivery profile of the light activated theranostic nanoagent.

3. Conclusions

Light-activated inflammatory cell ablation using a macrophage-avid nanoconstruct is a novel paradigm for the treatment of atherosclerosis, and has several potential advantages over other theranostic techniques. As compared to the nanoparticulate delivery of small molecule therapeutics, our systems are only toxic when activated by the appropriate wavelength of light, thereby minimizing off-target effects. As well, similar therapies could be envisioned using hyperthermia,[19] via the hysteresis heating of magnetic nanoparticles[20] or photothermal therapy with gold nanorods or nanoshells.[21] While these methodologies would limit extraneous toxicities, they suffer from lack of focal cell killing, as all healthy cells in the vicinity, including the vascular endothelial cells and smooth muscle cells, would also be subject to the increased temperatures, thereby causing extensive cell death. In the case of endothelial cell death, hyperthermia would make the lesion more rupture/thrombosis prone.

Aside from the ability of the nanoagent to affect focal macrophage ablation, it is also capable of functioning as a multimodal imaging agent for the detection of atherosclerotic lesions.[6,7] Clinically, the utility of fluorescence imaging is limited by the depth of penetration of light, although catheter-based systems are currently being developed for intravascular imaging.[22] Such a system would be capable of detecting our nanoagent within the vessel lumen with low light levels, and subsequently irradiating it with a therapeutic dose of light, using a “see and treat” approach. Although not utilized within this study, the nanoparticulate scaffold is also based upon superparamagnetic iron oxide, which is used clinically as a magnetic resonance imaging agent.[9,10] It may thus be possible to use the nanoagent to non-invasively detect inflamed, rupture prone lesions prior to the catheter-based intervention.

While the experiments contained within utilized a murine model in which the carotid artery is exposed in order to enable imaging and therapy, we also anticipate being able to perform this therapy non-invasively on some of the more superficial vasculature. In order to accomplish this feat, longer wavelength photosensitizers (> 750 nm) will likely be utilized to improve light penetration through tissue. In particular, non-invasive treatment of carotid artery lesions has the potential to reduce the incidence of stroke, a leading cause of death in the United States.[23]

We have thus engineered an improved near-infrared light activated theranostic nanoagent bearing spectrally distinct dyes for imaging and therapy, that is readily taken up by phagocytic macrophages and demonstrates superior phototoxicity compared to conventional chlorin agents. When utilized in vivo, the agent localizes to macrophage-rich regions within inflamed atherosclerotic lesions, and induces extensive apoptosis upon irradiation with a therapeutic dose of light. The measured skin phototoxcity was also substantially reduced, as compared to conventional photosensitizers. Overall, this study preliminarily demonstrates the viability of near infrared light activated therapeutic nanoagents in the treatment of atherosclerotic vascular disease. Future efforts will elucidate the ability of this methodology to induce a durable, macrophage-attenuated, plaque-stabilizing effect.

4. Experimental Section

General

All chemicals and solvents were purchased from Fisher or Sigma Aldrich and used as received without further purification. Silica gel (Sorbent Technologies, 60 Å, 40–63 μm, 230 × 400 mesh) was used for column chromatography. UV-vis spectra were recorded on a Varian Cary 50 UV-vis spectrophotometer. Fluorescence data were collected from a Varian Cary Eclipse fluorescence spectrophotometer. Absorption and fluorescence spectra were collected in DMF at room temperature unless noted otherwise. The absorption plate reader utilized was a Tecan Safire. LCMS data were collected form a Water 2695 HPLC equipped with a 2996 diode array detector, a Micromass ZQ4000 ESI-MS module, and a Grace-Vydac RPC18 column (model 218TP5210) at a flow rate of 0.3 mL/min. Gradients were run with buffer A (H_2O/0.1% trifluoroacetic acid (TFA)) and buffer B (90% acetonitrile/10% H_2O/0.1% TFA). For analytical HPLC a C-18 reverse phase column (Varian) was used with dimensions of 250 mm × 4.6 mm. For semi-preparative HPLC a C-18 reverse phase column (Varian) was used with dimensions of 250 mm × 21.2 mm. High-resolution electrospray ionization (ESI) mass spectra were obtained from a Bruker Daltonics APEXIV 4.7 T Fourier transform ion cyclotron resonance spectrometer (FT-ICR-MS) in the Department of Chemistry Instrumentation Facility (DCIF) at the Massachusetts Institute of Technology. All ^{1}H NMR spectra (500 MHz) and ^{13}C NMR spectra (125 MHz) were collected in the solvents noted. Particle size measurements were performed on a Malvern Zetasizer Nano. Crosslinked dextran-coated iron oxide nanoparticles (35 nm hydrodynamic radius) were obtained from the chemistry core at the Center for Molecular Imaging Research.[11] *meso*-tetra(*m*-methoxyphenyl)porphyrin[24] and fluorenylmethyl-protected glutaric acid, **Fm-Glu**[15] were synthesized as described previously. The procedure for singlet oxygen quantum yields determinations has been reported.[25]

5-(4-amino-3-methoxyphenyl)-10,15,20-tri(3-methoxyphenyl)porphyrin, 3

To a stirring solution of **1** (1.50 g, 2.04×10^{-3} mol) in 150 mL trifluoroacetic acid was added sodium nitrite (257 mg, 1.8 eq). The reaction was allowed to proceed for 4 min, at which time it was poured into 1500 mL distilled water. The resulting precipitate was filtered through Celite to remove the majority of the water, redissolved in CH_2Cl_2/MeOH (9:1), dried over anhydr $MgSO_4$, and evaporated to dryness under reduced pressure to give the crude nitrated product **2**. The resulting solid was then dissolved in conc HCl (150 mL) and heated to 60 °C under inert atmosphere while stirring. To this solution was added $SnCl_2 \oplus 2H_2O$ (3.67 g, 8 equiv). The reaction proceeded for 3 h at which time it was quenched by pouring the solution into 1500 mL distilled H_2O, and neutralization with conc NH_4OH. The resulting precipitate was filtered through Celite to remove the majority of the water, redissolved in CH_2Cl_2/MeOH (9/1), dried over anhydr $MgSO_4$, and evaporated to dryness under reduced pressure. The product was purified by flash chromatography (CH_2Cl_2, silica gel). All fractions containing the product were combined, evaporated to dryness, redissolved in CH_2Cl_2, and crystallized by slow solvent exchange into MeOH to give **3** as a purple microcrystalline powder in 51 % yield (0.67 g). A fraction containing the starting material **1** was also recovered (0.39 g, 26 %). UV-vis (DMF) λ_{max} (log ε): 426 (5.4), 518 (4.0), 560 (4.1), 599 (3.8), 653 (3.3) nm; ^{1}H NMR (300 MHz, $CDCl_3$, δ) −2.73 (s, 2H), 4.01 (m, 12H), 4.18 (s, 2H), 7.11 (d, J = 7.8 Hz, 1H), 7.36 (m, 3H), 7.68 (m, 5H), 7.84 (m, 6H), 8.91 (br s, 6H), 9.00 (d, J = 4.8 Hz, 2H) ppm; ^{13}C NMR (100 MHz, $CDCl_3$, δ) 55.5. 55.8, 113.2, 113.6, 117.7, 119.4, 120.5, 127.7, 132.4, 135.8, 143.6, 145.6, 158.0 ppm; +ESI-MS (30 V, CH_3CN/0.1% TFA) m/z = 750.5 (MH^+).

Fluorenylmethyl-protected 4-[2-methoxy-4-(10,15,20-tri(3-methoxyphenyl)porphyrin-5-yl)-phenylcarbamoyl]-butyric acid, 4

To an 80 mL microwave reaction vessel was added **3** (0.38 g, 5.07×10^{-4} mol), dicyclohexylcarbodiimide (DCC, 0.63 g, 6 equiv), Fm-Glu (0.94 g, 6 equiv), and a $CHCl_3$/Pyridine solution (25 mL, 95:5). The resulting solution was subject to microwave irradiation while stirring, with the following settings: T = 100 °C, t = 30 min, P_{max} = off. Once the reaction had cooled, it was filtered to remove the resulting insoluble dicyclohexylurea (DCU), diluted with DMF (25 mL) and evaporated to dryness. In order to remove the excess Fm-Glu, which is of similar polarity to the product, the crude product was subject to column chromatography (CH_2Cl_2/MeOH/TFA, 98/1.5/0.5, silica gel). The fractions containing the crude product were combined and the total volume was reduced to 25 mL, at which point the TFA was neutralized by addition of 5 mL DMF/Et_3N (95/5). The resulting solution was evaporated to dryness, dissolved in EtOAc and washed thrice with water, dried over anhydr $MgSO_4$, and evaporated to dryness. The pure product was then dissolved in CH_2Cl_2 and precipitated with hexanes to yield **4** as a purple powder (0.48 g, 91%). UV-vis (DMF) λ_{max} (log ε): 421 (5.6), 515 (4.2), 552 (3.9), 591 (3.7), 647 (3.5) nm; ^{1}H NMR (500 MHz, $CDCl_3$, δ) −2.56 (s, 2H), 2.22 (m, 2H), 2.57 (m, 2H), 2.68 (m, 2H), 4.07 (s, 12H), 4.29 (m, 1H), 4.57 (d, *J* = 6.5 Hz, 2H), 7.47 (m, 8H), 7.72 (m, 6H), 7.82 (d, *J* = 7.0 Hz, 2H), 7.94 (m, 8H), 8.04 (d, *J* = 7.5 Hz, 1H), 8.84 (d, *J* = 7.5 Hz, 1H), 9.11 (m, 9H) ppm; ^{13}C NMR (125 MHz, $CDCl_3$, δ) 20.7, 33.4, 36.6, 47.0, 55.6, 56.1, 66.3, 113.5, 113.8, 117.1, 118.0, 119.9, 120.0, 120.1, 120.2, 120.6, 120.8, 125.1, 127.2, 127.5, 127.7, 127.8, 127.9, 128.0, 137.8, 141.4, 143.6, 143.8, 146.3, 158.1, 170.7, 173.2 ppm.

Fluorenylmethyl-protected 4-[2-methoxy-4-(2,3-dihydroxy-10,15,20-tri(3-methoxyphenyl)chlorin-5-yl)-phenylcarbamoyl]-butyric acid, 5I, and fluorenylmethyl-protected 4-[2-methoxy-4-(12,13-dihydroxy-10,15,20-tri(3-methoxyphenyl)chlorin-5-yl)-phenylcarbamoyl]-butyric acid, 5II

To a solution of **4** (191 mg, 1.8×10^{-4} mol) in CH_2Cl_2/pyridine (10 mL, 95/5) was added OsO_4 in CH_2Cl_2/pyridine (0.78 mL, 0.83 equiv, 0.05 g/mL). The reaction was allowed to proceed for 24 h, at which time it was diluted with DMF (10 mL), and evaporated to dryness. The crude product was then dissolved in CH_2Cl_2 and H_2S was bubbled through the reaction for 5 min, at which time the reaction was allowed to proceed for 45 min. The solution was evaporated to dryness, redissolved in CH_2Cl_2, filtered through celite, and evaporated to dryness. The products were purified by column chromatography (silica gel, CH_2Cl_2/MeOH (98/2)), and the fractions containing the respective isomer were combined and evaporated to dryness. The products were redissolved in CH_2Cl_2 and precipitated with hexanes to give isomer I (31 mg, 19%), and isomer II (36 mg, 22%).

5I

UV-vis (DMF) λ_{max} (log ε): 422 (5.3), 519 (4.2), 548 (4.1), 596 (3.8), 648 (4.4) nm; ^{1}H NMR (500 MHz, $CDCl_3$, δ) −1.76 (s, 2H), 2.18 (m, 2H), 2.56 (t, *J* = 6.5 Hz, 2H), 2.64 (t, *J* = 6.5 Hz, 2H), 3.28 (br s, 2H), 3.99 (m, 13H), 4.29 (t, *J* = 6.5 Hz, 1H), 4.53 (d, *J* = 6.5 Hz, 2H), 6.43 (d, *J* = 23.0 Hz, 2H), 7.31 (m, 3H), 7.38 (t, *J* = 7.0 Hz, 2 H), 7.46 (t, *J* = 7.0 Hz, 2H), 7.54 (d, *J* = 18.5 Hz, 2H), 7.73 (m, 14 H), 8.08 (s, 1H), 8.42 (d, *J* = 11.0 Hz, 2H), 8.57 (s, sH), 8.74 (br s, 3H) ppm; ^{13}C NMR (125 MHz, $CDCl_3$, δ) 20.7, 33.3, 36.6, 46.9, 55.5, 56.0, 66.3, 74.1, 74.3, 113.0, 113.4, 113.6, 113.8, 116.3, 116.5, 117.9, 118.5, 119.8, 120.1, 122.8, 122.9, 124.4, 125.1, 126.5, 127.2, 127.4, 127.6, 127.9, 128.2, 128.6, 128.8, 132.7, 135.6, 135.7, 137.2, 140.7, 141.4, 142.4, 143.2, 143.8, 146.2, 153.0, 153.2, 158.0, 158.7, 159.1, 161.4, 170.5, 173.2 ppm; +ESI-MS (30 V, CH_3CN/0.1% TFA) m/z = 1076.7 (MH^+).

5II

UV-vis (DMF) λ_{max} (log ε): 422 (5.4), 519 (4.1), 548 (4.1), 596 (3.9), 648 (4.4) nm; ^{1}H NMR (500 MHz, $CDCl_3$, δ) −1.78 (s, 2H), 2.16 (m, 2H), 2.53 (s, 2H), 2.62 (s, 2H), 3.99 (s, 13H), 4.28 (s, 1H), 4.52 (s, 2H), 6.42 (d, *J* = 21.5 Hz, 2H), 7.53 (m, 26H), 8.06 (s, 1H), 8.44 (s, 2H), 8.56 (s, 2H). 8.73 (m, 3H) ppm; ^{13}C NMR (125 MHz, $CDCl_3$, δ) 20.7, 33.3, 36.6, 46.9, 55.5, 56.1, 66.3, 74.1, 74.4, 113.0, 113.7, 113.8, 114.2, 116.3, 118.8, 120.1, 122.9, 124.2, 125.1, 126.7, 126.9, 127.2, 127.6, 127.9, 128.2, 132.7, 135.6, 136.6, 140.6, 140.9, 141.4, 142.3, 143.2, 143.8, 146.7, 153.1, 158.0, 170.5, 173.1 ppm; +ESI-MS (30 V, CH_3CN/0.1% TFA) m/z = 1076.7 (MH^+).

4-[2-hydroxy-4-(2,3-dihydroxy-10,15,20-tri(3-hydroxyphenyl)chlorin-5-yl)-phenylcarbamoyl]-butyric acid, 6I, and 4-[2-hydroxy-4-(12,13-dihydroxy-10,15,20-tri(3-hydroxyphenyl)chlorin-5-yl)-phenylcarbamoyl]-butyric acid, 6II

To a solution of **5I** or **5II** (31.1 mg, 2.9×10^{-5} mol) in anhydr CH_2Cl_2 (10 mL) under an argon atmosphere was added BBr_3 (300 μL, 1 M in CH_2Cl_2, 12 equiv). The reaction is allowed to proceed for 1 h, at which time it is quenched by addition of MeOH (5 mL), and neutralized with DMF/Et_3N (10 mL, 95/5). The solution was evaporated to dryness, dissolved in EtOAc, washed thrice with water, dried over anhydr $MgSO_4$, and evaporated to dryness. The crude product was then dissolved in DMF/piperidine (4:1) to effect deprotection of the fluorenylmethyl group, reacted for 20 min, and evaporated to dryness. The products were purified by HPLC (80% Buffer A to 20% Buffer A), with the fractions containing the pure product being combined and evaporated to dryness. The product was precipitated from *i*PrOH with hexanes to give the product in 31 % yield (9 mg).

6I

UV-vis (DMF) λ_{max} (log ε): 420 (5.1), 550 (3.9), 547 (3.9), 595 (3.6), 648 (4.2) nm; ^{1}H NMR (500 MHz, Methanol-d_4, δ) 2.02 (m, 2H), 2.36 (m, 2H), 2.55 (t, *J* = 7.5, 2H), 6.25 (m, 2H), 7.03 (d, *J* = 7.5, 1H), 7.10 (d, *J* = 7.5, 2H), 7.26 (m, 2H), 7.33 (m, 1H), 7.49 (m, 8H), 8.34 (d, *J* = 5.0, 1H), 8.40 (m, 3H), 8.63 (d, *J* = 5.0, 2H) ppm; ^{13}C NMR (125 MHz, Methanol-d_4, δ) 23.3, 36.3, 37.2, 75.4, 75.6, 115.0, 115.4, 115.5, 115.7, 116.0, 120.9, 121.8, 122.6, 123.1, 125.3, 126.7, 128.9, 129.0, 129.2, 129.5, 133.5, 136.6, 142.0, 142.1, 144.2, 144.5, 154.3, 157.2, 157.4, 157.8, 164.0, 164.3, 174.9, 175.2 ppm; +ESI-MS (30 V, CH_3CN/0.1% TFA) m/z = 842.5 (MH^+).

6II

UV-vis (DMF) λ_{max} (log ε): 421 (5.1), 520 (4.0), 548 (4.0), 596 (3.7), 648 (4.2) nm; ^{1}H NMR (500 MHz, Methanol-d_4, δ) 2.11 (t, *J* = 8.5 Hz, 2H). 2.47 (m, 2H), 2.65 (t, *J* = 8.5 Hz, 2H), 6.33 (d, *J* = 12.5 Hz, 2H), 7.11 (d, *J* = 8.0 Hz, 2H), 7.18 (d, *J* = 9.0 Hz, 1H), 7.33 (s, 2H), 7.57 (m, 9H), 8.01 (s, 1H), 8.42 (d, *J* = 6.0 Hz, 2H), 8.50 (d, *J* = 5.5 Hz, 1H), 8.53 (d, *J* = 6.0 Hz, 1H), 8.71 (d, *J* = 6.0 Hz, 1H), 8.75 (d, *J* = 6.0 Hz, 1H) ppm; ^{13}C NMR (125 MHz, Methanol-d_4, δ) 21.6, 34.3, 35.7, 74.1, 113.9, 114.0, 114.2, 114.5, 119.4, 120.7, 121.9, 123.7, 125.5, 127.5, 127.7, 128.0, 132.0, 135.1, 135.2, 139.0, 140.5, 142.7, 143.0, 146.8, 152.9, 155.7, 156.0, 156.3, 162.5, 173.4 ppm; +ESI-MS (30 V, CH_3CN/0.1% TFA) m/z = 842.5 (MH^+).

General synthesis of succinimidyl esters of 6I or 6II

To **6I** or **6II** (~10 mg) in DMF (5 mL) was added DCC (4 equiv), 4-dimethylaminopyridine (0.4 equiv), and N-hydroxysuccinimide (4 equiv). The reaction was allowed to proceed for 2 h, at which time the solution was filtered through a plug of cotton and evaporated to dryness. The solid was then dissolved in anhydr DMSO (2 mL) and filtered through a plug of cotton

to remove any residual solid. The resulting solution was used for conjugation to the nanoparticle without purification.

Dye labelling of CLIO

To 20 mg CLIO (12.12 mg Fe mL^{-1}) in PBS was added AlexaFluor 750 (1 mg, Molecular Probes, Eugene, OR). The reaction was allowed to proceed for 16 h, at which time the suspension was filtered through Sephadex G-25 to give **CLIO-AF750**. The resultant solution was divided, with one half kept as the control agent, and the remainder reacted with the chlorin. To **CLIO-AF750** (10 mg) was added **7I** (2 mg) dissolved in anhydr DMSO (300 μL). The reaction was allowed to proceed for 16 h, at which time it was filtered through Sephadex G-25 to give the final product, **CLIO-THPC**. The number of dyes per particle was determined as described previously.[14]

Cellular uptake and phototoxicity

Murine macrophage RAW 264.7 cells growing in DMEM media were resuspended in PBS and incubated with **CLIO-THPC**, **CLIO-AF750**, or chlorin e6 at varying concentrations (50nM-5μM) for 3 hours. Cells were then washed with fresh media. At this point, selected cells were examined by fluorescence microscopy (Nikon TE2000, Nikon Instruments Inc.) by light microscopy and utilizing rhodamine (ex/em 546/590) and Cy7 (ex/em 710/810) filter cubes. Selected cells for photodynamic therapy were illuminated with a 650 nm laser, 150 mW, 3 minutes for total fluence of 6 J/cm2. Cells were returned to the incubator overnight and then evaluated by MTS assay (CellTiter 96 AQueous One Solution Cell Proliferation Assay, Promega Corp.) for cell viability determination. MTS results were analyzed on a well plate reader (Tecan Saphire).

In vivo uptake and phototoxicity

Male $ApoE^{-/-}$ mice aged 23–29 weeks on high cholesterol diet since 13 weeks of age were injected with **CLIO-THPC** or **CLIO-AF750** (as a control) at a dose of 10 mg Fe/kg in PBS via tail vein injection. One day post-injection mice were anesthetized with ketamine/xylazine by peritoneal injection and the carotid artery was surgically exposed. Mice were imaged with an Olympus IV100 intravital laser scanning fluorescence microscope developed for imaging small experimental animals (Olympus Inc.). Images were obtained in the AF750 channel as well as the FITC channel to detect autofluorescence. Imaging was performed before and after injection of FITC-dextran (0.5mg, MW 2,000,000, 2 mg/mL, Invitrogen Corp.) to image the vessel lumen and aid with registration of images. Following imaging, carotid ateries were illuminated externally with a 650 nm laser, 150 mW, 1 cm target, 3 minutes for total fluence of 11 J/cm2. Mice were returned to their housing for 1 day. Following IVFM or apoptosis endpoints, mice were perfused with 20 mL of cold PBS and dissected. Specimens were embedded in OCT compound and stored at −80°C. Specimens were stained with hematoxylin and eosin, Mac-3 for macrophage content, and TUNEL peroxidase staining for apoptosis (Apoptag Peroxidase, Millipore Corp.). Percent TUNEL positive cells determined in ImageJ (NIH) after Color-based Thresholding. Cohorts: **CLIO-THPC** - 5 mice, **CLIO-AF750** - 5 mice

Mouse hind paw edema model

Female c57/bl6 mice were injected with **CLIO-THPC** at a dose of 10mg Fe/kg in PBS or chlorin e6 5mg/kg via tail vein injection. Baseline footpad thickness was measured bilaterally with a digital caliper. After a drug-light interval of 1 h or 24 h, the mice were anesthetized with inhaled isoflurane (2%) and the right footpad was illuminated with a 650 nm laser, 150 mW, 3 minutes for total fluence of 11 J/cm2. Repeat footpad measurements were performed 24 hours after light exposure. Footpad swelling was analyzed using the

change in footpad thickness as a percentage of baseline, using the left (non-illuminated) footpad as a control. Cohorts: **CLIO-THPC** - 1 h - 3 mice; 24 h - 3 mice, Chlorin e_6 - 1 h - 5 mice, 24 h - 3 mice.

Acknowledgments

We would like to thank Drs. Rainer Kohler and Jose-Luiz Figueiredo for their assistance with surgery and IVFM imaging, and Dr. Elena Aikawa and Yoshiko Iwamoto, B.S. for histopathology. Special thanks to Dr. Martha Morton for expertise and assistance with acquisition of NMR spectra. This work was supported in part by NIH grants R21HL093607 (JM), U01-HL080731 (JM, FJ, RW), the American Heart Association Scientist Development Grant (FJ), and the Howard Hughes Medical Institute Career Development Award (FJ).

References

1. Murray CJ, Lopez AD. Lancet. 1997; 349:1498–1504. [PubMed: 9167458]
2. Hansson GK. N Engl J Med. 2005; 352:1685–1695. [PubMed: 15843671]
3. Libby P. Nature. 2002; 420:868–874. [PubMed: 12490960]
4. Hansson GK, Libby P. Nat Rev Immunol. 2006; 6:508–519. [PubMed: 16778830]
5. Jaffer FA, Libby P, Weissleder R. Circulation. 2007; 116:1052–1061. [PubMed: 17724271]
6. Jaffer FA, Nahrendorf M, Sosnovik D, Kelly KA, Aikawa E, Weissleder R. Mol Imaging. 2006; 5:85–92. [PubMed: 16954022]
7. Nahrendorf M, Zhang H, Hembrador S, Panizzi P, Sosnovik DE, Aikawa E, Libby P, Swirski FK, Weissleder R. Circulation. 2008; 117:379–387. [PubMed: 18158358]
8. Pande AN, Kohler RH, Aikawa E, Weissleder R, Jaffer FA. J Biomed Opt. 2006; 11:021009. [PubMed: 16674184]
9. Trivedi RA, UK-IJM, Graves MJ, Kirkpatrick PJ, Gillard JH. Neurology. 2004; 63:187–188. [PubMed: 15249641]
10. a) Kooi ME, Cappendijk VC, Cleutjens KB, Kessels AG, Kitslaar PJ, Borgers M, Frederik PM, Daemen MJ, van Engelshoven JM. Circulation. 2003; 107:2453–2458. [PubMed: 12719280] b) Trivedi RA, U-King-Im JM, Graves MJ, Cross JJ, Horsley J, Goddard MJ, Skepper JN, Quartey G, Warburton E, Joubert I, Wang L, Kirkpatrick PJ, Brown J, Gillard JH. Stroke. 2004; 35:1631–1635. [PubMed: 15166394] c) Trivedi RA, Mallawarachi C, U-King-Im JM, Graves MJ, Horsley J, Goddard MJ, Brown A, Wang L, Kirkpatrick PJ, Brown J, Gillard JH. Arterioscler Thromb Vasc Biol. 2006; 26:1601–1606. [PubMed: 16627809]
11. Josephson L, Tung CH, Moore A, Weissleder R. Bioconjug Chem. 1999; 10:186–191. [PubMed: 10077466]
12. a) McCarthy JR, Kelly KA, Sun EY, Weissleder R. Nanomedicine (Lond). 2007; 2:153–167. [PubMed: 17716118] b) McCarthy JR, Weissleder R. Adv Drug Deliv Rev. 2008; 60:1241–1251. [PubMed: 18508157]
13. a) Kereiakes DJ, Szyniszewski AM, Wahr D, Herrmann HC, Simon DI, Rogers C, Kramer P, Shear W, Yeung AC, Shunk KA, Chou TM, Popma J, Fitzgerald P, Carroll TE, Forer D, Adelman DC. Circulation. 2003; 108:1310–1315. [PubMed: 12939212] b) Rockson SG, Kramer P, Razavi M, Szuba A, Filardo S, Fitzgerald P, Cooke JP, Yousuf S, DeVault AR, Renschler MF, Adelman DC. Circulation. 2000; 102:2322–2324. [PubMed: 11067782] c) Rockson SG, Lorenz DP, Cheong WF, Woodburn KW. Circulation. 2000; 102:591–596. [PubMed: 10920074]
14. McCarthy JR, Jaffer FA, Weissleder R. Small. 2006; 2:983–987. [PubMed: 17193154]
15. Griffin JH, Linsell MS, Nodwell MB, Chen Q, Pace JL, Quast KL, Krause KM, Farrington L, Wu TX, Higgins DL, Jenkins TE, Christensen BG, Judice JK. J Am Chem Soc. 2003; 125:6517–6531. [PubMed: 12785792]
16. a) Brückner C, Dolphin D. Tetrahedron Lett. 1995; 36:9425–9428. b) Brückner C, Dolphin D. Tetrahedron Lett. 1995; 36:3295–3298.
17. a) Aikawa E, Nahrendorf M, Sosnovik D, Lok VM, Jaffer FA, Aikawa M, Weissleder R. Circulation. 2007; 115:377–386. [PubMed: 17224478] b) Jaffer FA, Kim DE, Quinti L, Tung CH,

Aikawa E, Pande AN, Kohler RH, Shi GP, Libby P, Weissleder R. Circulation. 2007; 115:2292–2298. [PubMed: 17420353]

18. Peng Q, Warloe T, Moan J, Godal A, Apricena F, Giercksky KE, Nesland JM. Cancer Res. 2001; 61:5824–5832. [PubMed: 11479222]
19. Gordon RT, Hines JR, Gordon D. Med Hypotheses. 1979; 5:83–102. [PubMed: 459972]
20. a) Han HD, Choi MS, Hwang T, Song CK, Seong H, Kim TW, Choi HS, Shin BC. J Pharm Sci. 2006; 95:1909–1917. [PubMed: 16795016] b) Ponce AM, Viglianti BL, Yu D, Yarmolenko PS, Michelich CR, Woo J, Bally MB, Dewhirst MW. J Natl Cancer Inst. 2007; 99:53–63. [PubMed: 17202113] c) Sonvico F, Mornet S, Vasseur S, Dubernet C, Jaillard D, Degrouard J, Hoebeke J, Duguet E, Colombo P, Couvreur P. Bioconjug Chem. 2005; 16:1181–1188. [PubMed: 16173796]
21. a) Gobin AM, Lee MH, Halas NJ, James WD, Drezek RA, West JL. Nano Lett. 2007; 7:1929–1934. [PubMed: 17550297] b) Hirsch LR, Stafford RJ, Bankson JA, Sershen SR, Rivera B, Price RE, Hazle JD, Halas NJ, West JL. Proc Natl Acad Sci U S A. 2003; 100:13549–13554. [PubMed: 14597719]
22. a) Calfon MA, Vinegoni C, Ntziachristos V, Jaffer FA. J Biomed Opt. 2010; 15:011107. [PubMed: 20210433] b) Jaffer FA, Vinegoni C, John MC, Aikawa E, Gold HK, Finn AV, Ntziachristos V, Libby P, Weissleder R. Circulation. 2008; 118:1802–1809. [PubMed: 18852366]
23. Kung HC, Hoyert DL, Xu J, Murphy SL. Natl Vital Stat Rep. 2008; 56:1–120. [PubMed: 18512336]
24. Banfi S, Caruso E, Caprioli S, Mazzagatti L, Canti G, Ravizza R, Gariboldi M, Monti E. Bioorg Med Chem. 2004; 12:4853–4860. [PubMed: 15336264]
25. McCarthy JR, Perez JM, Bruckner C, Weissleder R. Nano Lett. 2005; 5:2552–2556. [PubMed: 16351214]

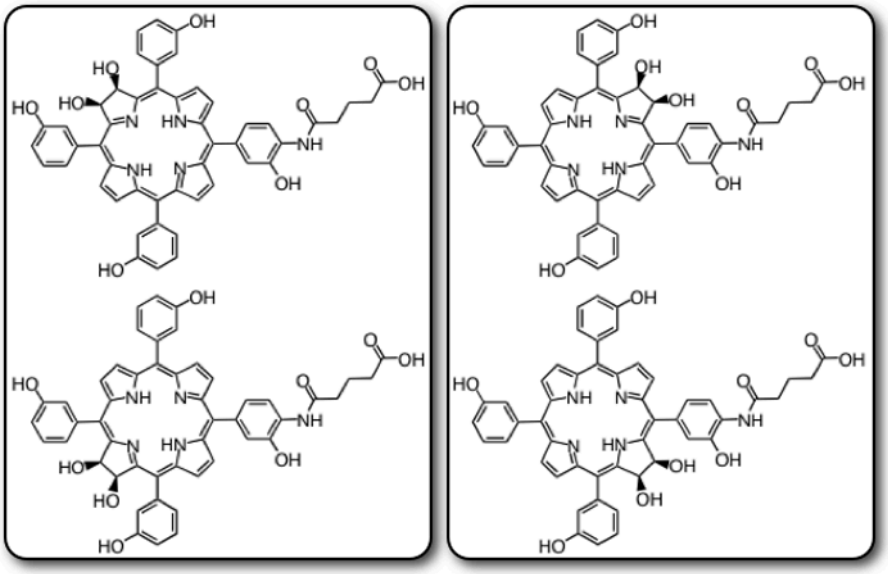

Figure 1.

Four isomers are synthesized via the OsO_4-mediated dihydroxylation of porphyrin **4**. They are separable by column chromatography into regioisomers as depicted in the boxes above for compound **6**. The Roman number designation refers to the least polar (**I**) and more polar (**II**) stereoisomers.

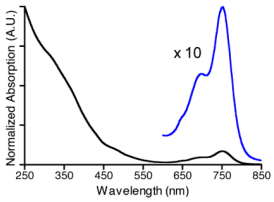

Figure 2.
UV-vis absorption spectrum of **CLIO-THPC**. An expansion (10 ×) of the region between 600 nm and 850 nm is depicted in blue.

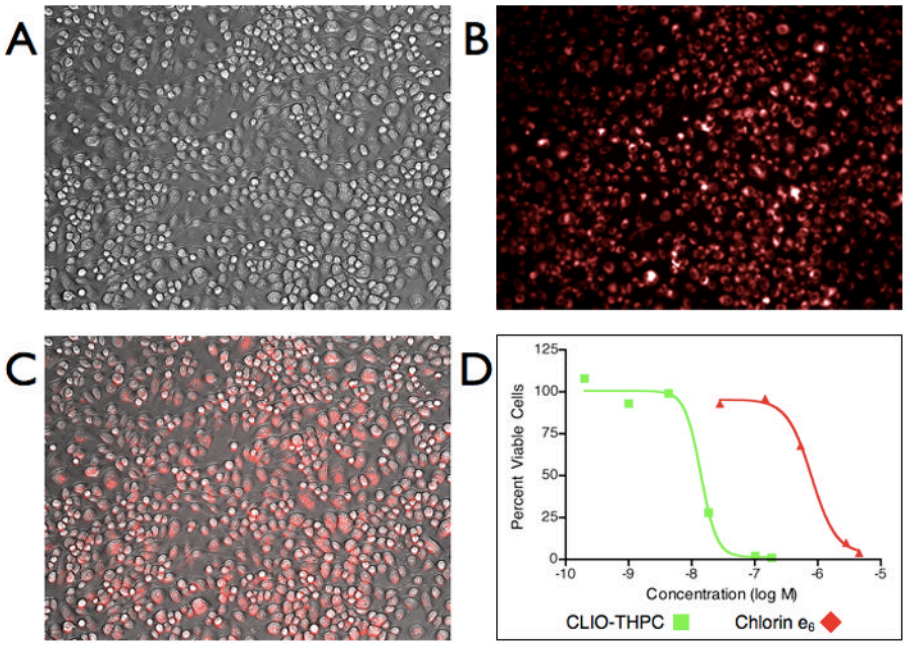

Figure 3.

Cellular uptake and phototoxicity of **CLIO-THPC**. A) Brightfield microscopic image of RAW 264.7 murine macrophages (20×); B) Fluorescent microscopic image of nanoagent uptake in the rhodamine channel (20×); C) Merge of the brightfield and fluorescence channels illustrating localization; D) Phototoxicity of **CLIO-THPC** versus chlorin e_6 (650 nm, 50 mW cm^{-2}).

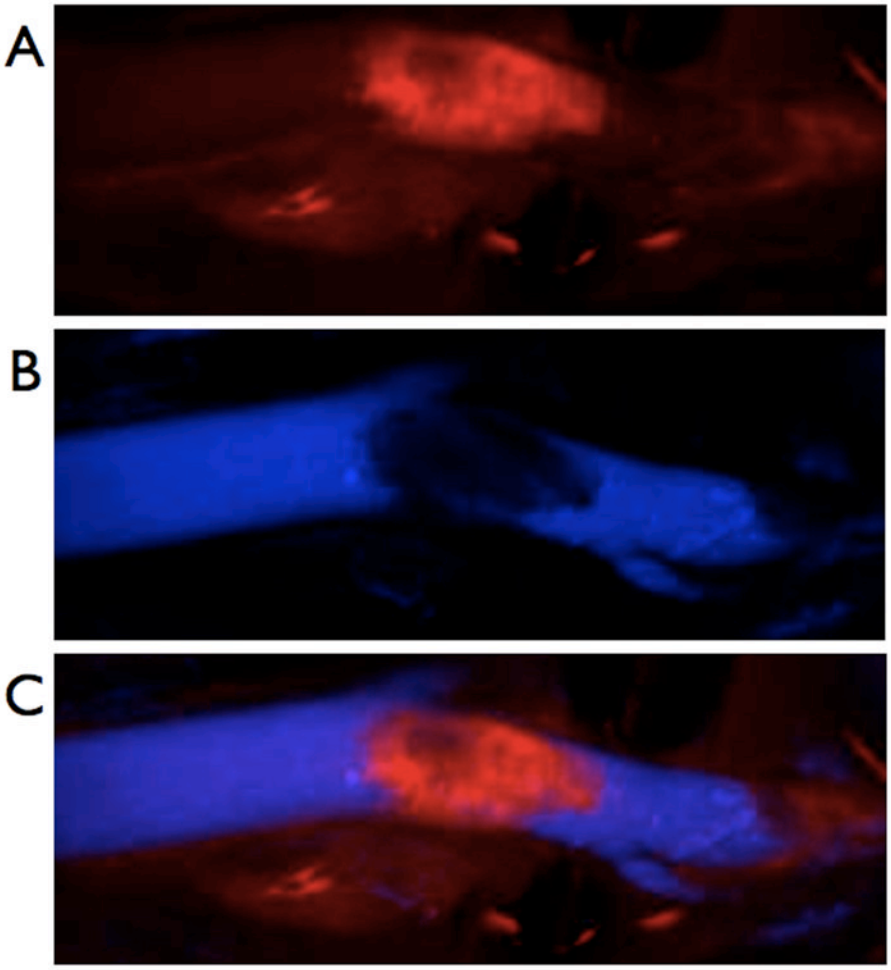

Figure 4.

In vivo localization of the nanoagent, **CLIO-THPC**, to carotid atheroma, as determined by intravital fluorescence microscopy. A) Fluorescence image in the AF750 channel demonstrating particle uptake by a carotid plaque. B) Fluorescence angiogram utilizing fluorescein-labeled dextran outlining the vasculature. C) Merged image of the two fluorescence channels.

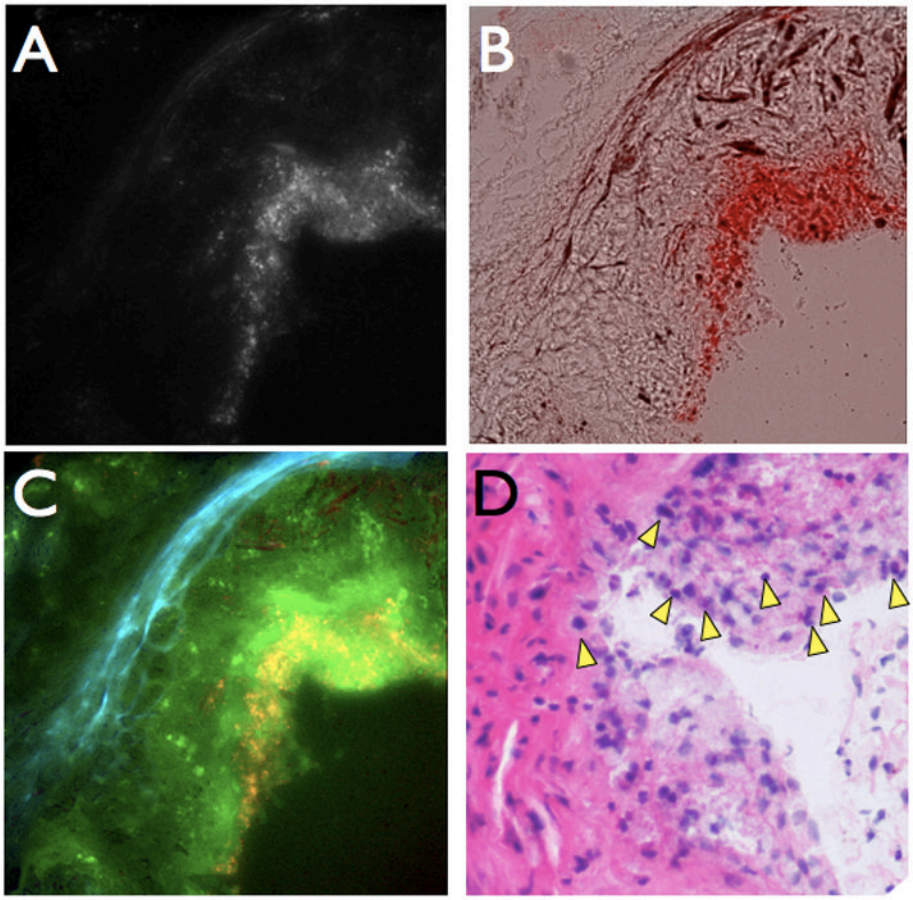

Figure 5.

CLIO-THPC localizes in atheroma in apoE$^{-/-}$ mice. Fluorescence microscopy of an aortic root plaque section, 24 hours after agent injection (A) at 750 nm excitation shows strong subendothelial deposition from the AF750 moiety, as further evident on (B) the brightfield-750 nm merged image. (C) Three color merge of **CLIO-THPC** deposition in atheroma, with elastin autofluroescence (blue, 510 nm filter), THPC (green, 680 nm filter), and AF750 (red, 750 nm filter) demonstrating agent deposition (yellow and bright green areas) is distinct from autofluorescence (blue elastin fiber signals). (D) An adjacent section revealed several pyknotic cells with condensed nuclei consistent with plaque apoptosis/death (H&E image, ×200, arrowheads).

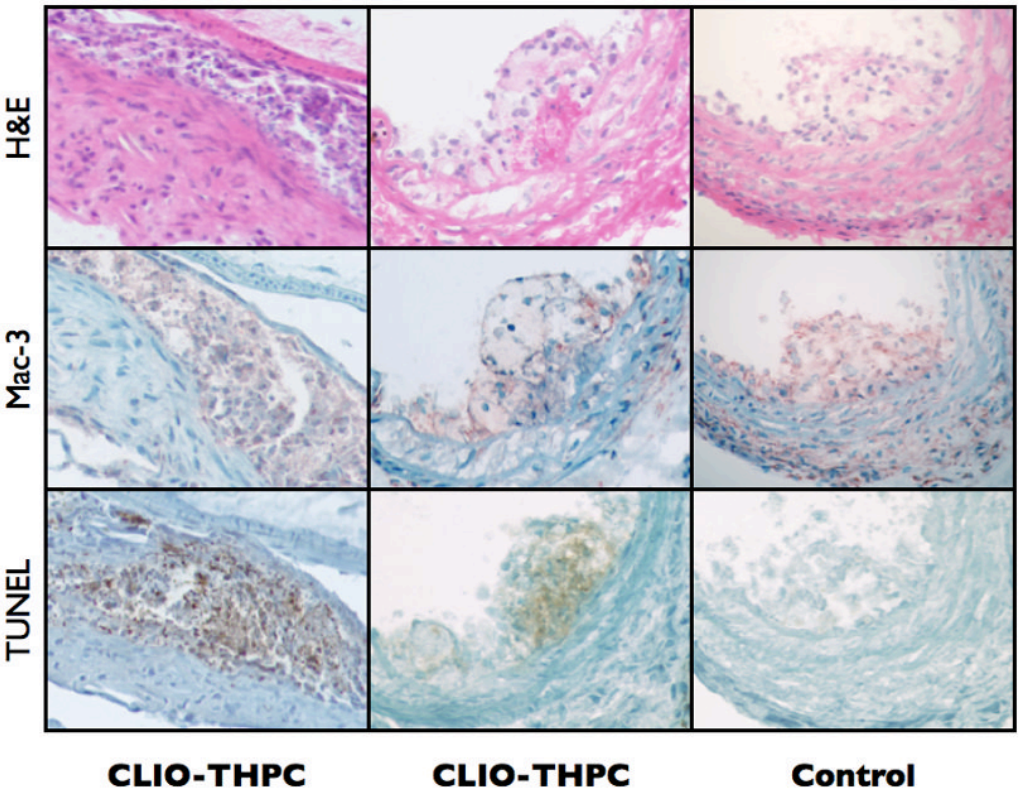

Figure 6.

At 24 h post therapy, **CLIO-THPC** injected mice showed extensive macrophage cell death (left two columns) and apoptosis in atheroma (lower panels, TUNEL stain). Minimal cell injury was present in laser light-exposed plaques of the **CLIO-AF750** control group (right column), or in non-irradiated contralateral plaques from **CLIO-THPC** (data not shown).

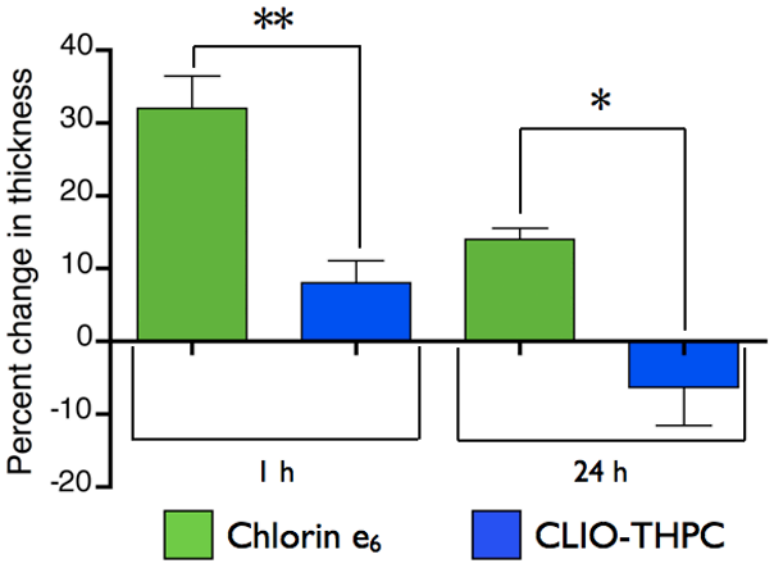

Figure 7.

Skin photosensitivity of chlorin e_6 versus **CLIO-THPC** based upon a hind paw edema model. Edema is measured as a change in thickness in the treated paw 24 hours after laser irradiation. (** $P = 0.009$, * $P = 0.02$)

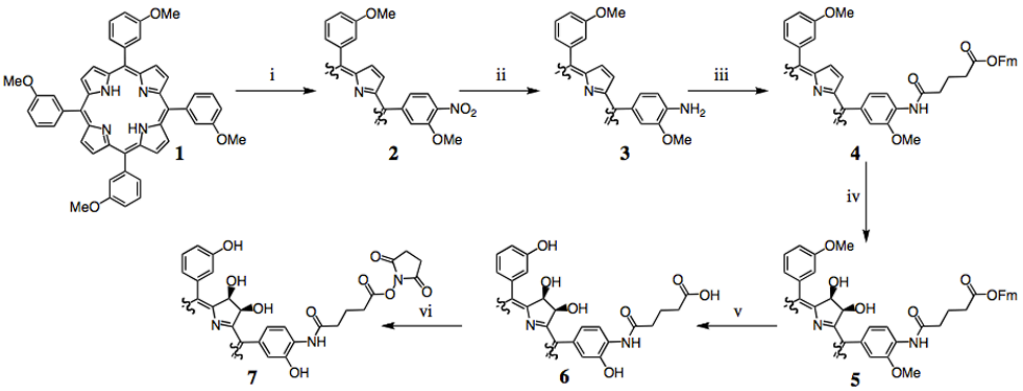

Scheme 1.

Synthesis of conjugatable *meso*-tetra(hydroxyphenyl)chlorin derivatives. i) 1.8 equiv $NaNO_2$/TFA; ii) $SnCl_2 \cdot 2H_2O$, HCl; iii) **Fm-Glu**, DCC; iv) 1. OsO_4, 2. H_2S; v) 1. BBr_3, 2. Pipiridine/DMF (1:4); vi) NHS, DCC, DMAP.